Published in final edited form as:

Mol Carcinog. 2018 November ; 57(11): 1458–1466. doi:10.1002/mc.22869.

Knockout of Human Arylamine *N*-Acetyltransferase 1 (NAT1) in MDA-MB-231 Breast Cancer Cells Leads to Increased Reserve Capacity, Maximum Mitochondrial Capacity, and Glycolytic Reserve Capacity

Samantha M. Carlisle[1], **Patrick J. Trainor**[2], **Mark A. Doll**[1], **Marcus W. Stepp**[1], **Carolyn M. Klinge**[3], and **David W. Hein**[1]

[1]Department of Pharmacology and Toxicology, University of Louisville School of Medicine, Louisville, Kentucky, USA 40202

[2]Division of Cardiovascular Medicine, University of Louisville School of Medicine, Louisville, Kentucky, USA 40202

[3]Department of Biochemistry and Molecular Genetics, University of Louisville School of Medicine, Louisville, Kentucky, USA 40202

Abstract

Introduction: Human arylamine *N*-acetyltransferase 1 (NAT1) is a phase II xenobiotic metabolizing enzyme found in almost all tissues. NAT1 can also hydrolyze acetyl-coenzyme A (acetyl-CoA) in the absence of an arylamine substrate. Expression of NAT1 varies between individuals and is elevated in several cancers including estrogen receptor positive (ER+) breast cancers. To date however, the exact mechanism by which NAT1 expression affects mitochondrial bioenergetics in breast cancer cells has not been described.

Methods: To further evaluate the role of NAT1 in energy metabolism MDA-MB-231 breast cancer cells with parental, increased, and knockout levels of NAT1 activity were compared for bioenergetics profile. Basal oxygen consumption rate (OCR) and extracellular acidification rate (ECAR) were measured followed by programmed sequential injection of Oligomycin (ATP synthase inhibitor), FCCP (ETC uncoupler), Antimycin A (Complex III inhibitor) and Rotenone (Complex I inhibitor) to evaluate mitochondrial bioenergetics.

Results: Compared to the cell lines with parental NAT1 activity, NAT1 knockout MDA-MB-231 cell lines exhibited significant differences in bioenergetics profile, while those with increased NAT1 did not. Significant increases in reserve capacity, maximum mitochondrial capacity, and glycolytic reserve capacity were observed in NAT1 knockout MDA-MB-231 cell lines compared to those with parental and increased NAT1 activity.

Corresponding Author: Samantha M. Carlisle, Kosair Charities CTR, RM 352A, 505 South Hancock Street, Louisville, KY 40202, USA, Telephone: 502-852-6284, (no fax number), samantha.carlisle@louisville.edu.

Authors' contributions: SMC, DWH, and CMK participated in research design. SMC conducted experiments. MAD and MWS contributed new reagents or analytic tools. SMC, CMK, and PJT performed data analysis. SMC, CMK, MWS, DWH, and PJT contributed to the writing of the manuscript.

Competing interests: The authors declare that they have no competing interests.

Conclusions: These data indicate that NAT1 knockout in MDA-MB-231 breast cancer cells may enhance adaptation to stress by increasing plasticity in response to energy demand.

Keywords

arylamine *N*-acetyltransferase 1; NAT1; Breast Cancer; MDA-MB-231; Bioenergetics

1 Introduction

Human arylamine *N*-acetyltransferase 1 (NAT1) is classically described as a phase II xenobiotic metabolizing enzyme that can catalyze both the deactivation and bioactivation of certain environmental arylamine carcinogens using acetyl coenzyme A [1–3]. More recently, NAT1 has also been shown to catalyze the hydrolysis of acetyl coenzyme A (acetyl-CoA) in the absence of an arylamine substrate using folate as a cofactor [4,5] however the implications of this reaction in metabolism and bioenergetics are undefined (reviewed in [6]). NAT1 expression varies inter-individually and is commonly elevated in several cancers including estrogen receptor positive (ER+) breast cancers [7]. A 2009 microarray study of 56 breast tumor samples and 10 normal tissue samples revealed NAT1 expression was higher in invasive carcinoma compared with normal tissue [8,9]. Computational analysis of a previously published microarray dataset containing 89 breast cancer samples also revealed that NAT1 is commonly amplified in breast carcinomas [10,11]. Comparative proteomic analysis of 8 normal breast samples and 25 breast cancer derived tissues demonstrated that NAT1 is elevated in invasive ductal carcinoma (IDC) and invasive lobular carcinoma (ILC) when compared to normal breast tissue [12]. Overexpression of NAT1 in the conditionally immortalized HB4a human mammary luminal epithelial cell line leads to increased cell growth and resistance to the chemotherapeutic etoposide [12]. Additionally, knockdown of NAT1 in the MDA-MB-231 triple negative breast cancer cell line, through both small molecule inhibition and siRNA, leads to decreased cell growth, and metastatic and invasive abilities ([13–15]; reviewed in [16]). However, the exact mechanism by which NAT1 expression affects breast cancer risk and progression has yet to be described.

Recent studies have demonstrated that congenic rats expressing higher NAT2 (orthologous to human NAT1) activity exhibited more carcinogen-induced mammary tumors, independent of carcinogen metabolism [17]. Notably, endogenous acetyl-CoA was shown to be decreased in MDA-MB-231 cells with increased NAT1 activity when compared to the MDA-MB-231 cell line with parental NAT1 activity [18]. Investigation of the polar metabolome of the same cells also revealed statistically significant differences in a number of metabolites, including amino acids and palmitoleic acid [18].

These observations, along with NAT1's extensive tissue distribution [19], presence in nearly every species [20], and ability to catalyze the hydrolysis of acetyl-CoA [4,5], lead us to hypothesize that NAT1's role in cancer may be related to regulation of acetyl-CoA. Recently, NAT1 was postulated to have an endogenous role in the methionine salvage pathway, but this role was not observed in MDA-MB-231 cells since they do not have a functional methionine salvage pathway due to a lack of methylthioadenosine phosphorylase (MTAP) activity [21]. To further investigate the hypothesis that NAT1 can influence the

levels of acetyl-CoA thus leading to downstream effects on mitochondrial bioenergetics, we constructed MDA-MB-231 triple negative breast cancer (TNBC) cell lines that vary only in NAT1 activity. The MDA-MB-231 cell line was chosen because it expresses an approximate mid-level of NAT1 RNA when compared to other breast cancer cell lines [22]. Selecting a single breast cancer cell line and manipulating the level of NAT1 in that single cell line has allowed us to evaluate the effect of both increased and knockout NAT1 expression in a breast cancer cell line model that has the same genetic background. This method eliminates confounding mutations that would be present when using multiple breast cancer cell lines that innately express varying levels of NAT1 thus making interpretations about NAT1's role more straightforward.

Since NAT1 has been reported to hydrolyze acetyl-CoA [4,5] and acetyl-CoA is a central molecule in cellular bioenergetics, we interrogated differences in the cellular bioenergetics of the genetically engineered MDA-MB-231 cells that vary only in NAT1. This approach allowed us to further examine NAT1 for possible downstream effects on energy metabolism. Functional metabolic analysis of live cells was examined using Seahorse XF technology (reviewed in [23]). Programmed sequential injection of compounds that inhibit specific portions of the electron transport chain (ETC) were utilized to probe different measurements of mitochondrial function.

2 Materials and Methods

To evaluate the effect of differing levels of NAT1 expression on the bioenergetics profile of triple negative breast cancer cells we utilized parental and 4 constructed MDA-MB-231 cell lines in this study (5 cell lines total). Previously constructed and characterized MDA-MB-231 breast cancer cell lines expressing parental (*Parent*, *Scrambled*) and increased (*Up*) levels of human arylamine *N*-acetyltransferase 1 (NAT1) were used as samples [13,18]. The *Scrambled* cell line was included as a transfection control. Additionally, newly constructed cell lines expressing no detectable (knockout) NAT1 activity (*CRISPR 2–19, CRISPR 5–50*) were used as samples (Fig. 1). All cell lines, including newly constructed CRISPR/Cas9 generated cell lines, were authenticated by the ATCC Short Tandem Repeat (STR) profiling cell authentication service.

2.1 Construction of CRISPR/Cas9 Cell Lines

The complete NAT1 knockout cell lines utilized within this study were constructed from MDA-MB-231 cells that had an FRT site inserted and had previously been transfected with a scrambled shRNA (referred to as the *Scrambled* cell line) to allow direct comparison to a single cell line regardless of the method used to construct the cell line. All cell lines were cultured in high-glucose Dulbecco's Modified Eagle Medium (DMEM), with 10% fetal bovine serum, 5% glutamine, and 5% penicillin/streptomycin added and grown in a humidified incubator set at 37 °C with 5% CO_2. Horizon Discovery Group (Waterbeach, United Kingdom) designed 5 different guide RNAs (gRNAs) specific for NAT1 and DNA2.0 Inc. (Newark, CA) cloned the gRNAs into a Cas9 expressing vector that also expressed a dasher-GFP tag. Separately, each of the 5 gRNA/Cas9 vectors were transiently transfected in the *Scrambled* MDA-MB-231 cell line using the Amaxa Nucleofector II (Lonza, Allendale,

NJ). Forty-eight hours after transfection cells were harvested and DNA isolated. The Transgenomic Inc. (Omaha, NE) SURVEYOR Mutation Detection Kit was used to determine the effectiveness of each gRNA's ability to cut the genomic DNA and induce DNA strand breaks effectively. gRNAs #2 and #5 were the most effective at inducing DNA strand breaks, and were chosen to separately knockout the function of NAT1 in the following studies.

The *Scrambled* MDA-MB-231 cell line was transfected with either #2 or #5 gRNA/Cas9 vectors as described above. Forty-eight hours after transfection cells were sorted for GFP fluorescence. The fluorescent positive cells were collected and plated at very dilute cell concentrations so that individual clones could be isolated. Once individual cells had grown into large enough colonies (several weeks), cloning cylinders were utilized to isolate those colonies using trypsin to release them from the plate and transferred to a 96-well culture plate. Clones were passaged until there were enough cells to plate in a 10 cm dish. Cells were then tested for NAT1 activity as previously described [24]. Activity assays showed NAT1 activity was not detectable (knocked out) in a low number of clones and these clones were selected for further characterization. Clones with no detectable NAT1 activity were further screened by sequencing the NAT1 open reading frame (ORF). We were specifically interested in clones that had deleted/inserted nucleotides in the NAT1 ORF that resulted in frame-shift mutations and thus premature protein termination signals resulting in predicted nonfunctional NAT1. Individual knockout cell lines representing the knockout of NAT1 activity for gRNA #2 or #5 were chosen based on NAT1 enzymatic activity and genomic sequence. Further details on NAT1 knockout cell line construction and characterization are described elsewhere [25].

2.2 Characterization of Constructed Cell Lines

In vitro NAT1 *N*-acetylation activity was determined in all cell lines included in this study. Briefly, suitably diluted cell lysate from each cell line was incubated with 1 mM acetyl-CoA and 300 μM *p*-aminobenzoic acid (PABA) at 37°C for 10 minutes. Reactions were terminated with the addition of 1/10 reaction volume 1 M acetic acid. Reaction products were collected and analyzed using an Agilent Technologies 1260 Infinity high performance liquid chromatography (HPLC) using a LiChrospher ® 100 RP-18 (5 μm) column to quantitate acetylated product. Differences in NAT1 *N*-acetylation between cell lines were tested by one-way ANOVA followed by Bonferroni post-tests.

Cell doubling times for the *Scrambled* & *Up* cell lines have been described previously [13]. Cell doubling times for newly constructed CRISPR/Cas 9 cell lines (*CRISPR 2–19* & *CRISPR 5–50*) were calculated as follows. Twenty-five thousand cells were plated in triplicate in 6-well plates and allowed to grow for 5 consecutive days. Cells were plated on day 1 and allowed to equilibrate for 24 h before making the first count on day 2 followed by counts on days 3, 4, 5 and 6 using a cell counter. The cell doubling time was calculated as previously described [13]. This assay was performed in triplicate for each cell line.

2.3 Mitochondrial Bioenergetics

The Seahorse XF24 Analyzer (Agilent Technologies, Santa Clara, CA) was utilized to interrogate differences in mitochondrial cellular metabolism via oxygen consumption rate (OCR) and extracellular acidification rate (ECAR) measurements of live cells. All cell lines were cultured in high-glucose Dulbecco's Modified Eagle Medium (DMEM), with 10% fetal bovine serum, 5% glutamine, and 5% penicillin/streptomycin added.

Twenty-four hours prior to each bioenergetics experiment, 100 μL of cell suspension from each cell line was plated in quadruplicate in a 24-well Seahorse XF24 cell culture microplate at a density of 40,000 cells per well, thus giving four biological replicates for each cell line. Additionally, four wells contained medium only for background correction purposes. To minimize the edge effects of plating and to ensure a monolayer of cells was formed on the bottom of the well, microplates were left in the cell culture hood at room temperature for one hour before being placed in a 37°C, 5% CO_2 incubator. After cells had adhered to the plate (three hours after placing in the incubator), 150 μL of medium was added to each well and cells were allowed to grow overnight. One hour prior to the experiment, medium was aspirated from each well and replaced with 675 μL Seahorse running medium. Seahorse running medium consisted of 8.3 grams/liter of Dulbecco's Modified Eagle's Medium (DMEM) base without glucose, L-glutamine, phenol red, sodium pyruvate and sodium bicarbonate (Sigma, St. Louis, MO), and 1.85 g NaCl per liter, glucose added to a final concentration of 25 mM, sodium pyruvate added to a final concentration of 1 mM, and 10 mL/liter of 100 x Glutamax-1 added, all at pH 7.4. Microplates were then incubated for one hour in a non-CO_2 37°C incubator. The XF24 sensor cartridge was hydrated overnight in XF calibrant solution in a non- CO_2 37°C incubator.

Before each experiment, solutions of compounds to be loaded in the ports of the sensor cartridge were freshly made from stock solutions. Chosen compounds inhibit specific portions of the mitochondrial electron transport chain to allow the elucidation of several different measurements of mitochondrial function [26]. Seventy-five microliters of 15 μM Oligomycin (ATP synthase inhibitor) was loaded into port A of the sensor cartridge, eighty-three microliters of 5 μM carbonyl cyanide-*p*-trifluoromethoxyphenylhydrazone (FCCP; mitochondrial inner membrane uncoupler) was loaded into port B of the sensor cartridge, and ninety-two microliters of 10 μM Antimycin A (complex III inhibitor) and 2 μM Rotenone (complex I inhibitor) was loaded into port C of the sensor cartridge. For background correction wells seahorse running media was loaded into each port in place of the compound solutions. The sensor cartridge was then loaded into the Seahorse XF24 analyzer and calibrated. Once calibration of the sensor cartridge was complete, the microplate was loaded into the machine and the experiment was started. Timed sequential injections of Oligomycin, FCCP, and Antimycin A/Rotenone occurred at 35, 50, and 64 minutes, respectively.

Six independent experiments were conducted. Each experiment consisted of four biological replicates for each of the cell lines. Baseline OCR, Baseline ECAR, Baseline OCR/ECAR, ATP-Linked OCR, Reserve Capacity, Coupling Efficiency, Proton Leak, Glycolytic Reserve, Maximum Mitochondrial Capacity, and Non-Mitochondrial Respiration were calculated as described in Table 1 following each experiment [26,27]. Results from each independent

experiment were summarized as mean ± SEM from four biological replicates on the microplate. Results from all six independent experiments were then complied with final results represented as mean ± SEM. One-way ANOVA was conducted for each measurement to test for overall differences, followed by multiplicity adjusted post hoc tests on only those measurements that were found to be significant.

2.4 MTT Cell Growth Assays

MTT (3-(4,5-Dimethylthiazol-2-yl)-2,5-Diphenyltetrazolium Bromide) assays were conducted in triplicate to determine if there were differences in cell viability between the cell lines given that the cells were allowed to grow in the plate for 24 hours prior to bioenergetics measurements. Cells were plated in the Seahorse XF24 plates following the same procedure that was used when plating cells for bioenergetics experiments. Instead of measuring the bioenergetics of the cells 24 hours after plating, media was removed from each well and cells were incubated with 250 μL of 5 mg/mL MTT dissolved in growth medium in a 37°C, 5% CO_2 incubator. After one hour, the media was aspirated and 250 μL of dimethyl sulfoxide (DMSO) was added to each well to solubilize the MTT. The microplate was gently rocked for 10 minutes and then the resulting solution in each well was transferred to a 96-well plate. Absorbance was measured at 570 nm using the Gen5 microplate reader (BioTek Instruments Inc., Winooski, VT). All absorbance values were within the linear range of MTT. Absorbance measurements were median-scaled by plate to minimize between-day variance. Scaled absorbance values were tested for equivalence between cell lines. Equivalence was assessed using a two-one sided t-test (TOST) procedure that evaluated equivalence given a 20% margin.

2.5 Kaplan-Meier Analysis of NAT1 Transcript Expression on Relapse-Free Survival in 255 Patients With Triple Negative Breast Cancer Tumors

Kaplan-Meier Plotter [28], an online survival analysis tool, was utilized to interrogate the effect of NAT1 transcript expression (Affymetrix probe ID: 200004_at) on relapse-free survival in patients with primary triple negative breast cancer tumors. Triple negative breast cancer tumors were specifically chosen for this evaluation since the studies described here utilize a TNBC cell line. Evaluated data were from 255 ER-/PR-/HER2- (TNBC) breast tumors in the Kaplan-Meier Plotter database. Patients were split by median into low and high NAT1 expression groups (n=128 and n=127, respectively). Hazard ratio (HR), 95% confidence intervals, and logrank *P* were calculated.

3 Results

NAT1 *N*-acetylation activity was significantly ($p<0.05$) higher in the *Up* cell line by approximately 7-fold while the *CRISPR 2–19* and *CRISPR 5–50* cell lines had no detectable activity (Fig. 2). The *Parent* and *Scrambled* cell lines showed no significant ($p>0.05$) difference in NAT1 *N*-acetylation activity. No significant differences were observed in doubling time of the cell lines utilized in this study. The doubling times for the *Parent*, *CRISPR 2–19*, and *CRISPR 5–50* cell lines were 30.5 ± 1.0, 29.3 ± 1.1, and 29.8 ± 0.7 hours, respectively (n=3). The doubling times for the *Scrambled* and *Up* cell lines have been previously reported at 27.4 and 23.4 hours, respectively [13].

Although NAT1 is overexpressed in breast tumors [7,8,10–12] and catalyzes the hydrolysis of acetyl-CoA, the impact of NAT1 inactivation or overexpression on cellular bioenergetics has yet to be reported. We examined glucose oxidation and mitochondrial bioenergetics in MDA-MB-231 TNBC cells constructed to knockout or overexpress NAT1 and compared OCR and ECAR in these cells to the parental MDA-MB-231 cells by extracellular flux analysis. A summary of ANOVA *p*-values for each measurement are presented in Table 1. We did not observe an effect of modulation of NAT1 activity in MDA-MB-231 cells on basal OCR, ATP-linked OCR, or non-mitochondrial respiration ($p>0.05$ for all; Table 1).

Knockout of NAT1 activity increased reserve capacity and maximum mitochondrial capacity when compared to the cell lines with parental (*Parent, Scrambled*) and increased (*Up*) NAT1 activity ($p<0.05$ for all; Fig. 2). In the *Parent*, *Scrambled*, and *Up* cell lines the maximal respiration was lower than the basal OCR measurements resulting in a negative value for the reserve capacity calculation; since reserve capacity cannot be negative biologically, we termed the reserve capacity measurements in these groups as 0. Reserve capacity was increased 91- and 50-fold in the *CRISPR 2–19* and *CRISPR 5–50* cell lines, respectively. The 1.8-fold increase in reserve capacity of the *CRISPR 2–19* cell line compared to the *CRISPR 5–50* cell line was also statistically significant. Maximum mitochondrial capacity of the *CRISPR 2–19* cell line was significantly increased 3.2-fold, 6.0-fold, and 5.4-fold, with respect to the *Parent*, *Scrambled* and *Up* cell lines. Maximum mitochondrial capacity of the *CRISPR 5–50* cell line was also significantly increased 2.5-fold, 4.7-fold, and 4.2-fold, with respect to the *Parent*, *Scrambled* and *Up* cell lines.

Proton leak was increased 1.8-fold in one of the NAT1 knockout (*CRISPR 2–19*) cell lines but only when compared to the cell line with increased (*Up*) NAT1 activity (Fig. 3). We cannot conclude that this effect is due to NAT1 knockout since we did not observe the same result in the other NAT1 knockout cell line (*CRISPR 5–50*).

Baseline ECAR was increased in the two NAT1 knockout cell lines compared to the cell line with parental (*Parent*) NAT1 activity (Fig. 4). Baseline ECAR in the *CRISPR 2–19* cell line was increased 2.1-fold, 1.8-fold, 1.6-fold, and 1.4-fold with respect to the *Parent*, *Scrambled*, *Up*, and *CRISPR 5–50* cell lines. Baseline ECAR in the *CRISPR 5–50* cell line was also increased 1.5-fold compared to the *Parent* cell line ($p<0.05$ for all).

In the NAT1 knockout cell lines glycolytic reserve was increased compared to the cell lines with parental (*Parent, Scrambled*) and increased (*Up*) NAT1 activity (Fig. 4). Glycolytic reserve of the *CRISPR 2–19* cell line was increased 3.8-fold, 9.0-fold, and 45-fold with respect to the *Parent*, *Scrambled* and *Up* cell lines. Similarly, glycolytic reserve of the *CRISPR 5–50* cell line was increased 3.8-fold, 9.2-fold, and 46-fold with respect to the *Parent*, *Scrambled* and *Up* cell lines ($p<0.05$ for all).

Transfection of the *Parent* cell line with the scrambled control showed no effect on baseline OCR/ECAR results. However, the cell line with increased NAT1 activity as well as one of the NAT1 knockout cell lines had decreased baseline OCR/ECAR relative to the *Parent* cell line (Fig. 3). Both the *Up* and *CRISPR 2–19* cell lines were decreased 1.7-fold with respect to the *Parent* cell line ($p<0.05$). We did not observe an effect of modulation of NAT1 activity

on coupling efficiency, also called coupling ratio, which is defined as (oligomycin-sensitive OCR)/(basal OCR) (Fig. 5). This result agrees with the data in Figure 3 showing that altering NAT1 activity had no effect on basal OCR or ATP-linked OCR in these cell lines.

Overall, it is important to note that the two cell lines with parental NAT1 activity (*Parent, Scrambled*) showed comparable results. The knockout of NAT1 in MDA-MB-231 cells led to differences in multiple bioenergetics measurements while the overexpression of NAT1 led to no significant ($p>0.05$) differences when compared to the cell lines expressing parental (*Parent, Scrambled*) NAT1 activity.

To rule out differences in cell growth rate between cell lines over the course of our experiments, an MTT assay was conducted and the equivalence of MTT absorbance values were evaluated. With the exception of the *Parent* to *Scrambled* comparison, there was sufficient evidence to assert equivalence ($p<0.05$) in each of the pairwise equivalence tests. The *Parent* to *Scrambled* equivalence test was marginally significant ($p = 0.065$). This data suggests that modulation of NAT1 activity does not affect MDA-MB-231 cell viability over the course of these experiments.

We note that no significant effect (logrank $P=0.52$) of NAT1 mRNA transcript expression on relapse-free survival in breast cancer patients with primary TNBC tumors was observed. The calculated HR was 1.15 with a confidence interval of 0.75 – 1.75.

4 Discussion

It has been previously reported that TNBC cell lines, including MDA-MB-231 cells, have profound metabolic changes characterized by decreased mitochondrial respiration and increased glycolysis when compared to breast cancer cell lines that are ER positive, PR positive, and/or HER2 positive [29]. Since the purpose of this study was to evaluate how increased and knockout levels of human NAT1 affected the cellular bioenergetics of MDA-MB-231 breast cancer cells, the *Parent* MDA-MB-231 (no genetic alterations or transfections) was used as a baseline comparison. The *Scrambled* cell line (the *Parent* MDA-MB-231 cell line with a FRT site added into the genome and a scrambled shRNA transfected into that FRT site) was included as a transfection control [18]. We did not observe a significant effect of the scrambled shRNA on cellular bioenergetics in MDA-MB-231 cells. The *Up* cell line (the *Parent* MDA-MB-231 cell line with a FRT site added into the genome and a plasmid overexpressing human NAT1 stably transfected into that FRT site) yields overexpression of NAT1 [18]. Finally, two complete NAT1 knockout cell lines (*CRISPR 2–19* and *CRISPR 5–50*) constructed using CRISPR/Cas9 technology (as described in the Methods section), were evaluated to verify that observed effects were due to differences in NAT1 as opposed to off-target effects caused by a specific guide-RNA. Therefore, we have concluded a result was due to the knockout of NAT1 only when the same trend was observed in both CRISPR/Cas9 constructed cell lines.

Knockout of NAT1 in MDA-MB-231 cells significantly altered the bioenergetics profile of the cells while increased NAT1 expression did not significantly alter the bioenergetics profile when compared to the *Parent* MDA-MB-231 cell line. Significant increases in reserve

capacity, maximum mitochondrial capacity, and glycolytic reserve were observed in both NAT1 knockout cell lines compared to cell lines expressing parental and increased NAT1 activity. While basal OCR was unaffected by altered NAT1 activity, baseline ECAR was significantly increased in NAT1 knockout cells, suggesting an increase in glycolysis.

Baseline OCR is an indicator of baseline mitochondrial respiration. ATP-linked OCR is the difference between OCR before and after ATP synthase is inhibited with oligomycin. This allows estimation of the OCR that is used to drive mitochondrial ATP synthesis and is largely set by the ATP demand of the cells [30]. Modulation of NAT1 expression did not alter baseline or ATP-linked OCR in MDA-MB-231 cells. This suggests NAT1 does not play a role in the ATP demand responses in the cells. Coupling efficiency is calculated as the fraction of baseline OCR used for ATP synthesis (ATP-linked OCR/baseline OCR) [31]. Coupling efficiency was also unaffected by modulation of NAT1 in MDA-MB-231 cells providing further evidence to support the conclusion that that NAT1 does not play a role in ATP demand responses in these cells.

Reserve capacity is the difference between the basal and maximal respiration of the mitochondria and is broadly an evaluation of a cells ability to respond to increased energy demands such as those found in rapidly dividing cancer cells [30]. Increases in reserve capacity, as observed in the NAT1 knockout cell lines, could reflect enhanced oxidative capacity, mitochondrial biogenesis, or increased substrate provision [30]. Reserve capacity does not explicitly implicate or identify molecular mechanisms of action since it is dependent upon multiple parameters. The significant increase in reserve capacity measured in the two NAT1 knockout cell lines appears to be driven by the increase in maximal respiration in those cell lines. Maximal respiration rate is primarily determined by substrate supply and oxidation [30]. This includes substrate transport across the mitochondrial membrane as well as rate controlling metabolic enzymes. Taken together, these results indicate NAT1 may have a role, either directly or through its influence on acetyl-CoA levels, in regulation of mitochondrial substrate transport or metabolism. One could speculate that knockdown of NAT1 increases acetyl-CoA thereby increasing substrate(s) for the TCA cycle which could increase mitochondrial reserve capacity. This hypothesis should be investigated in future studies.

Glycolytic reserve is the difference between oligomycin-induced ECAR and baseline ECAR and is a measure of the maximum rate of conversion of glucose to pyruvate or lactate that can be achieved acutely by a cell [32]. This measurement is an important parameter to evaluate in cancer cells since there is such an increased demand for energy precursors. Increases in glycolytic reserve, as we observed in the two NAT1 knockout cell lines, also indicate that these cells can respond better to these increased energy demands. Here we report that NAT1 knockout, using two guide RNAs, increased the glycolytic reserve in MDA-MB-231 cells. There have been many studies [9,14,33,34] investigating the inhibition of NAT1 with small molecule inhibitors as a possible way to decrease the cancerous and metastatic properties of malignant cells; however, our data suggests knockout of NAT1 may allow cells to increase glycolysis and use mitochondrial reserve.

Mitochondria facilitate cellular stress responses, including the response to hypoxia and the activation of programmed cell death via the release of pro-apoptotic molecules [35]. Differences in mitochondrial function between cells that express varying levels of NAT1 may play a role in cancer initiation or tumorigenesis by modulating these responses. It appears knockout of NAT1 allows cells to express more plasticity in terms of response to energy demand. Our data suggest that NAT1 may play a role in an unknown response mechanism that keeps cancer cells from hijacking the mitochondrial machinery to produce increased amounts of ATP that would be needed by cancer cells.

In conclusion, we have observed that differences in NAT1 activity, particularly the knockout of NAT1, significantly alters the bioenergetics profile of MDA-MB-231 triple negative breast cancer cells. Reserve capacity, maximal respiration, and glycolytic reserve capacity were increased in the NAT1 knockout cell lines. Increases in these measurements suggest that NAT1 knockout cells may be better able to respond to stress. These findings provide evidence that NAT1modifies cellular acetyl-CoA levels and mitochondrial bioenergetics. Further investigation into the specific role NAT1 is playing in regulating cellular metabolism and bioenergetics is needed, ongoing, and will best be investigated via a multidisciplinary approach.

Acknowledgments:

Results of this study represent partial fulfillment of Samantha M. Carlisle's PhD in Pharmacology and Toxicology from the University of Louisville.

Funding: Partially supported by USPHS grants T32-ES011564, R01-DK053220, & R25-CA134283.

List of Abbreviations:

NAT1	arylamine *N*-acetyltransferase 1
OCR	oxygen consumption rate
ECAR	extracellular acidification rate
FRT	flippase recognition target
Acetyl-CoA	acetyl-coenzyme A

References

1. Hein DW. Molecular genetics and function of NAT1 and NAT2: role in aromatic amine metabolism and carcinogenesis. Mutation research 2002;506–507:65–77.
2. Hein DW, Doll MA, Fretland AJ et al. Molecular genetics and epidemiology of the NAT1 and NAT2 acetylation polymorphisms. Cancer epidemiology, biomarkers & prevention : a publication of the American Association for Cancer Research, cosponsored by the American Society of Preventive Oncology 2000;9(1):29–42.
3. Hein DW, Doll MA, Rustan TD et al. Metabolic activation and deactivation of arylamine carcinogens by recombinant human NAT1 and polymorphic NAT2 acetyltransferases. Carcinogenesis 1993;14(8):1633–1638. [PubMed: 8353847]

4. Stepp MW, Mamaliga G, Doll MA, States JC, Hein DW. Folate-Dependent Hydrolysis of Acetyl-Coenzyme A by Recombinant Human and Rodent Arylamine N-Acetyltransferases. Biochem Biophys Rep 2015;3:45–50. [PubMed: 26309907]

5. Laurieri N, Dairou J, Egleton JE et al. From arylamine N-acetyltransferase to folate-dependent acetyl CoA hydrolase: impact of folic acid on the activity of (HUMAN)NAT1 and its homologue (MOUSE)NAT2. PloS one 2014;9(5):e96370. [PubMed: 24823794]

6. Butcher NJ, Li P, Wang L, Minchin RF. Human Arylamine N-Acetyltransferase Type 1 In: Laurieri N, Sim E, editor. Arylamine N-Acetyltransferases in Health and Disease: World Scientific Publishing; 2018 p 91–107.

7. Abba MC, Hu Y, Sun H et al. Gene expression signature of estrogen receptor alpha status in breast cancer. BMC genomics 2005;6:37. [PubMed: 15762987]

8. Casey T, Bond J, Tighe S et al. Molecular signatures suggest a major role for stromal cells in development of invasive breast cancer. Breast cancer research and treatment 2009;114(1):47–62. [PubMed: 18373191]

9. Butcher NJ, Minchin RF. Arylamine N-acetyltransferase 1: a novel drug target in cancer development. Pharmacological reviews 2012;64(1):147–165. [PubMed: 22090474]

10. Chin K, DeVries S, Fridlyand J et al. Genomic and transcriptional aberrations linked to breast cancer pathophysiologies. Cancer cell 2006;10(6):529–541. [PubMed: 17157792]

11. Yuan Y, Curtis C, Caldas C, Markowetz F. A sparse regulatory network of copy-number driven gene expression reveals putative breast cancer oncogenes. IEEE/ACM transactions on computational biology and bioinformatics / IEEE, ACM 2012;9(4):947–954.

12. Adam PJ, Berry J, Loader JA et al. Arylamine N-acetyltransferase-1 is highly expressed in breast cancers and conveys enhanced growth and resistance to etoposide in vitro. Molecular cancer research : MCR 2003;1(11):826–835. [PubMed: 14517345]

13. Stepp MW, Doll MA, Carlisle SM, States JC, Hein DW. Genetic and small molecule inhibition of arylamine N-acetyltransferase 1 reduces anchorage-independent growth in human breast cancer cell line MDA-MB-231. Molecular carcinogenesis 2018;57(4):549–558. [PubMed: 29315819]

14. Tiang JM, Butcher NJ, Minchin RF. Small molecule inhibition of arylamine N-acetyltransferase Type I inhibits proliferation and invasiveness of MDA-MB-231 breast cancer cells. Biochemical and biophysical research communications 2010;393(1):95–100. [PubMed: 20100460]

15. Tiang JM, Butcher NJ, Minchin RF. Effects of human arylamine N-acetyltransferase I knockdown in triple-negative breast cancer cell lines. Cancer Med 2015;4(4):565–574. [PubMed: 25627111]

16. Laurieri N, Egleton JE, Russell AJ Human Arylamine N-Acetyltransferase Type 1 and Breast Cancer In: Sim EaL N, editor. Arylamine N-Acetyltransferases in Health and Disease: World Scientific Publishing; 2018 p 351–384.

17. Stepp MW, Doll MA, Samuelson DJ, Sanders MA, States JC, Hein DW. Congenic rats with higher arylamine N-acetyltransferase 2 activity exhibit greater carcinogen-induced mammary tumor susceptibility independent of carcinogen metabolism. BMC cancer 2017;17(1):233. [PubMed: 28359264]

18. Carlisle SM, Trainor PJ, Yin X et al. Untargeted polar metabolomics of transformed MDA-MB-231 breast cancer cells expressing varying levels of human arylamine N-acetyltransferase 1. Metabolomics : Official journal of the Metabolomic Society 2016;12(7):1–12.

19. Boukouvala S, Fakis G. Arylamine N-acetyltransferases: what we learn from genes and genomes. Drug metabolism reviews 2005;37(3):511–564. [PubMed: 16257833]

20. Vagena E, Fakis G, Boukouvala S. Arylamine N-acetyltransferases in prokaryotic and eukaryotic genomes: a survey of public databases. Current drug metabolism 2008;9(7):628–660. [PubMed: 18781915]

21. Witham KL, Minchin RF, Butcher NJ. Role for human arylamine N-acetyltransferase 1 in the methionine salvage pathway. Biochemical pharmacology 2017;125:93–100. [PubMed: 27865712]

22. Carlisle SM, Hein DW. Retrospective analysis of estrogen receptor 1 and N-acetyltransferase gene expression in normal breast tissue, primary breast tumors, and established breast cancer cell lines. Int J Oncol 2018In Press.

23. Kalyanaraman B, Cheng G, Hardy M et al. A review of the basics of mitochondrial bioenergetics, metabolism, and related signaling pathways in cancer cells: Therapeutic targeting of tumor

mitochondria with lipophilic cationic compounds. Redox biology 2018;14:316–327. [PubMed: 29017115]

24. Leff MA, Epstein PN, Doll MA et al. Prostate-specific human N-acetyltransferase 2 (NAT2) expression in the mouse. The Journal of pharmacology and experimental therapeutics 1999;290(1): 182–187. [PubMed: 10381774]
25. Stepp MW. Role of Human Arylamine N-acetyltransferase 1 in Tumorigenesis and Cancer Biology [Doctoral dissertation]: University of Louisville; 2017.
26. Dranka BP, Benavides GA, Diers AR et al. Assessing bioenergetic function in response to oxidative stress by metabolic profiling. Free radical biology & medicine 2011;51(9):1621–1635. [PubMed: 21872656]
27. Radde BN, Ivanova MM, Mai HX, Salabei JK, Hill BG, Klinge CM. Bioenergetic differences between MCF-7 and T47D breast cancer cells and their regulation by oestradiol and tamoxifen. The Biochemical journal 2015;465(1):49–61. [PubMed: 25279503]
28. Gyorffy B, Lanczky A, Eklund AC et al. An online survival analysis tool to rapidly assess the effect of 22,277 genes on breast cancer prognosis using microarray data of 1,809 patients. Breast cancer research and treatment 2010;123(3):725–731. [PubMed: 20020197]
29. Pelicano H, Zhang W, Liu J et al. Mitochondrial dysfunction in some triple-negative breast cancer cell lines: role of mTOR pathway and therapeutic potential. Breast cancer research : BCR 2014;16(5):434. [PubMed: 25209360]
30. Divakaruni AS, Paradyse A, Ferrick DA, Murphy AN, Jastroch M. Analysis and interpretation of microplate-based oxygen consumption and pH data. Methods in enzymology 2014;547:309–354. [PubMed: 25416364]
31. Brand MD, Nicholls DG. Assessing mitochondrial dysfunction in cells. The Biochemical journal 2011;435(2):297–312. [PubMed: 21726199]
32. Mookerjee SA, Nicholls DG, Brand MD. Determining Maximum Glycolytic Capacity Using Extracellular Flux Measurements. PloS one 2016;11(3).
33. Duval R, Xu X, Bui LC et al. Identification of cancer chemopreventive isothiocyanates as direct inhibitors of the arylamine N-acetyltransferase-dependent acetylation and bioactivation of aromatic amine carcinogens. Oncotarget 2016;7(8):8688–8699. [PubMed: 26840026]
34. Russell AJ, Westwood IM, Crawford MH et al. Selective small molecule inhibitors of the potential breast cancer marker, human arylamine N-acetyltransferase 1, and its murine homologue, mouse arylamine N-acetyltransferase 2. Bioorganic & medicinal chemistry 2009;17(2):905–918. [PubMed: 19059786]
35. Sabharwal SS, Schumacker PT. Mitochondrial ROS in cancer: initiators, amplifiers or an Achilles' heel? Nature reviews Cancer 2014;14(11):709–721. [PubMed: 25342630]

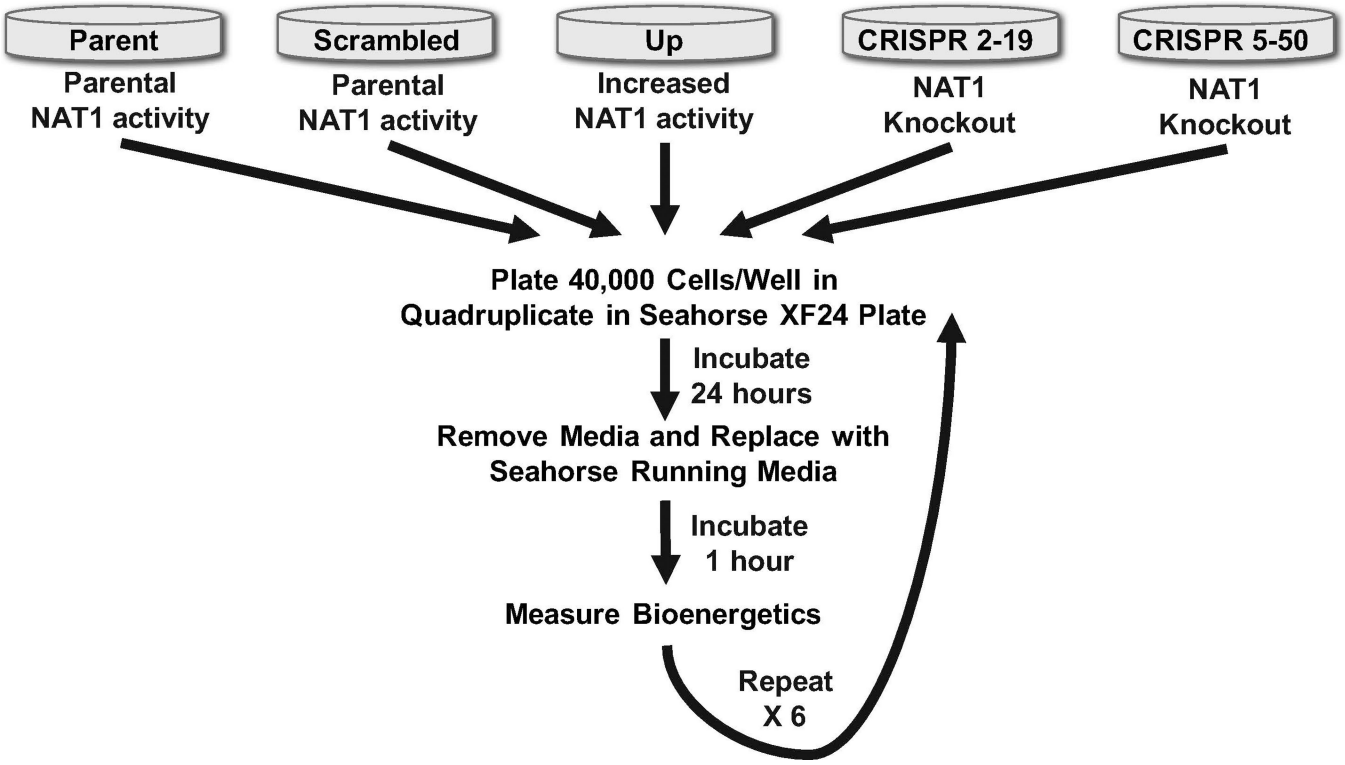

Figure 1: Diagram of Experimental Approach

Mitochondrial bioenergetics of five constructed MDA-MB-231 cell lines stably transformed to differ only in human arylamine *N*-acetyltransferase 1 (NAT1) were measured. The *Parent* and *Scrambled* cell lines express parental NAT1 activity, the *Up* cell line expresses increased NAT1 activity, and the *CRISPR 2–19* and *CRISPR 5–50* cell lines express no detectable NAT1 activity (knockout). Bioenergetics were measured in six independent experiments with four biological replicates of each cell line in each experiment.

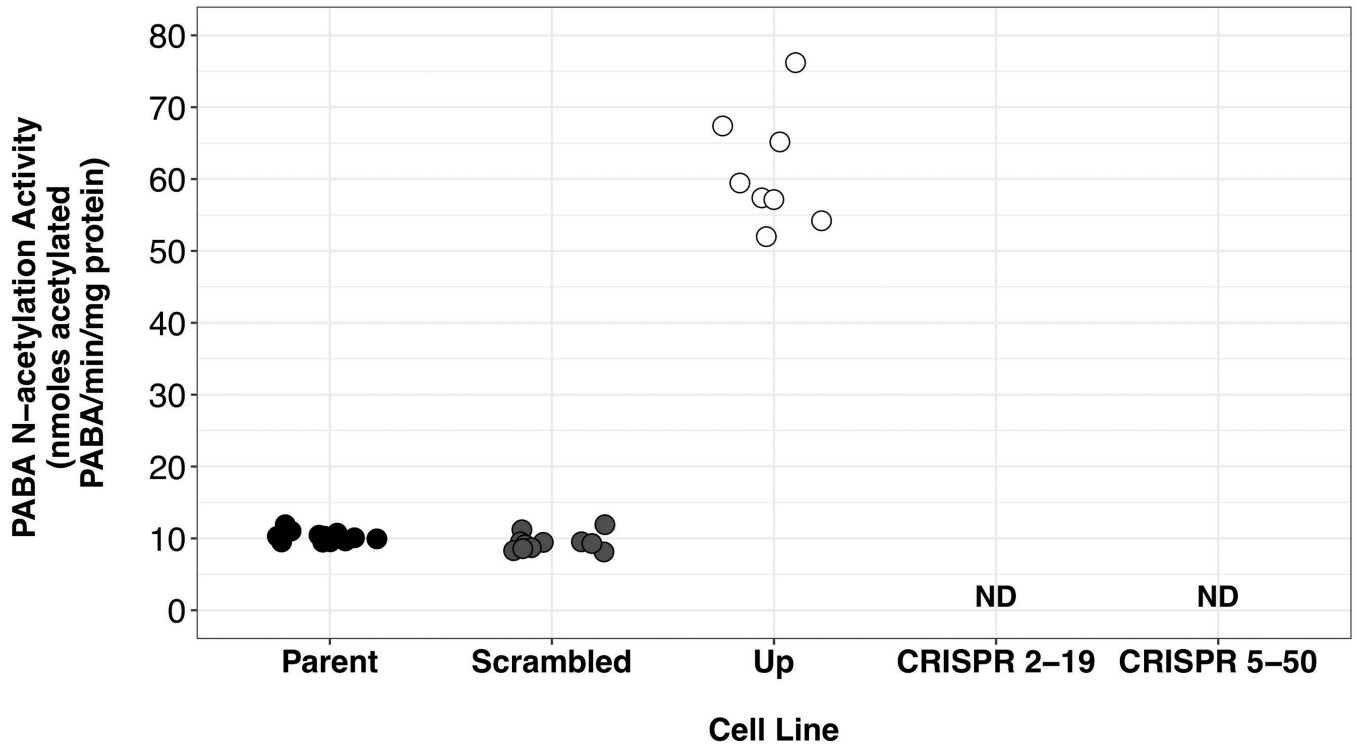

Figure 2: PABA *N*-acetylation Activity

PABA *N*-acetylation activity was measured via high-performance liquid chromatography in the 5 cell lines included in this study. *N*-acetylation activity of the *Parent* and *Scrambled* cell lines was not significantly (p>0.05) different. *N*-acetylation activity in the *Up* cell line was approximately 7-fold higher compared to the *Parent* and *Scrambled* cell lines. CRISPR/Cas 9 generated NAT1 knockout cell lines had no detectable *N*-acetylation activity.

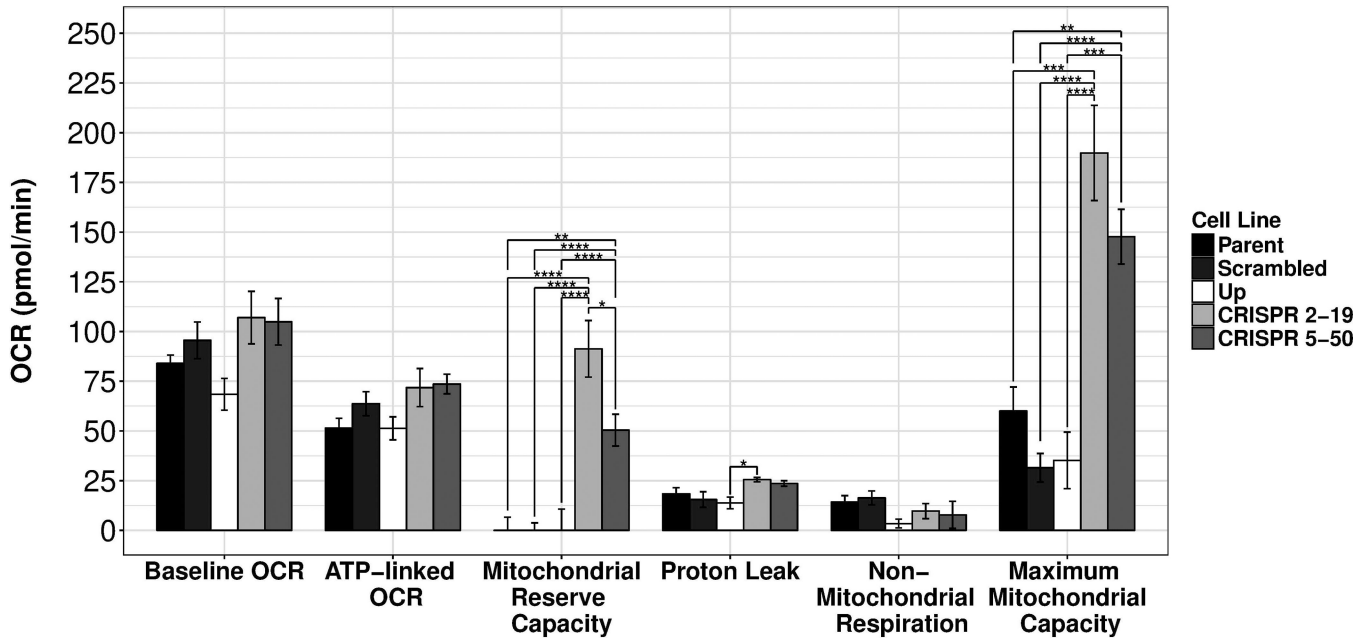

Figure 3: Oxygen Consumption Rate Bioenergetics Measures

Evidence of a difference in baseline oxygen consumption rate (OCR), ATP-linked OCR, and non-mitochondrial respiration across cell lines was not observed. Reserve capacity was significantly increased in the *CRISPR 2–19* and *CRISPR 5–50* cell lines when compared to the *Parent, Scrambled,* and *Up* cell lines. Reported reserve capacity measurements *for Parent, Scrambled,* and *Up* cell lines were truncated at 0 since reserve capacity cannot be negative. Proton leak was significantly increased in the *CRISPR 2–19* cell line but not the *CRISPR 5–50* cell line when compared to the *Up* cell line. Maximum mitochondrial capacity was significantly increased in the *CRISPR 2–19* and *CRISPR 5–50* cell lines when compared to the *Parent, Scrambled,* and *Up* cell lines. Order of bars are preserved throughout figure (*Parent, Scrambled, Up, CRISPR 2–19, CRISPR 5–50*) and represent mean ± SEM. N=6. *=p<0.05, **=p<0.01, ***=p<0.001, ****=p<0.0001. The *Parent* and *Scrambled* cell lines express parental NAT1 activity, the *Up* cell line expresses increased NAT1 activity, and the *CRISPR 2–19* and *CRISPR 5–50* cell lines express no NAT1 activity (knockout).

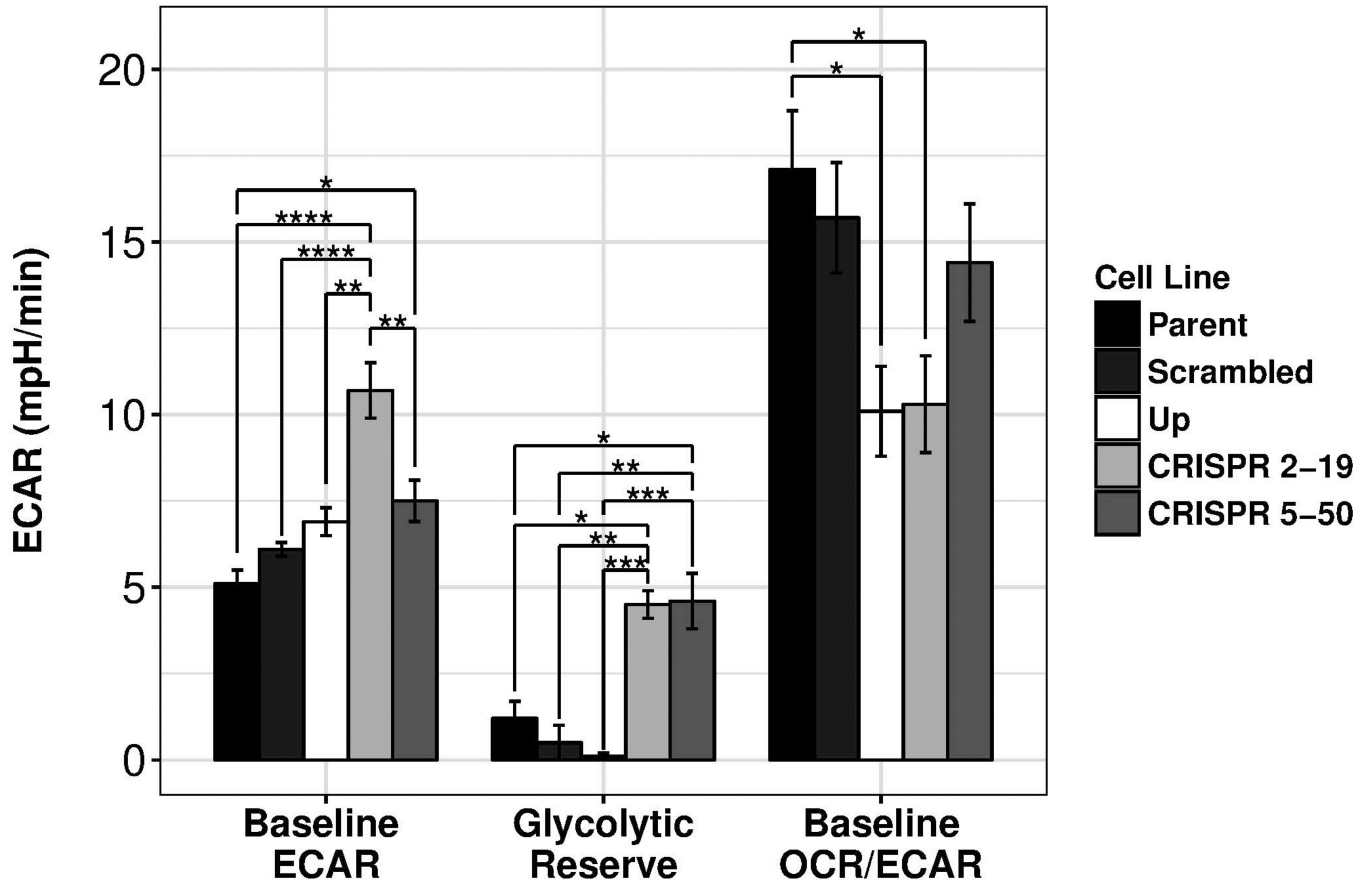

Figure 4: Extracellular Acidification Rate Bioenergetics Measures

Baseline extracellular acidification rate (ECAR) was significantly increased in the *CRISPR 2–19* cell line when compared to the *Parent*, *Scrambled*, *Up*, and *CRISPR 5–50* cell lines. The *CRISPR 5–50* cell line was also significantly increased compared to the *Parent* cell line. Glycolytic reserve capacity was significantly increased in the *CRISPR 2–19* and *CRISPR 5–50* cell lines compared to the *Parent, Scrambled,* and *Up* cell lines. Baseline OCR/ECAR was significantly decreased in the *Up* and *CRISPR 2–19* cell lines when compared to the *Scrambled* cell line. Order of bars are preserved throughout figure (*Parent, Scrambled, Up, CRISPR 2–19, CRISPR 5–50*) and represent mean ± SEM. N=6. *=p<0.05, **=p<0.01, ***=p<0.001, ****=p<0.0001. The *Parent* and *Scrambled* cell lines express parental NAT1 activity, the *Up* cell line expresses increased NAT1 activity, and the *CRISPR 2–19* and *CRISPR 5–50* cell lines express no NAT1 activity (knockout).

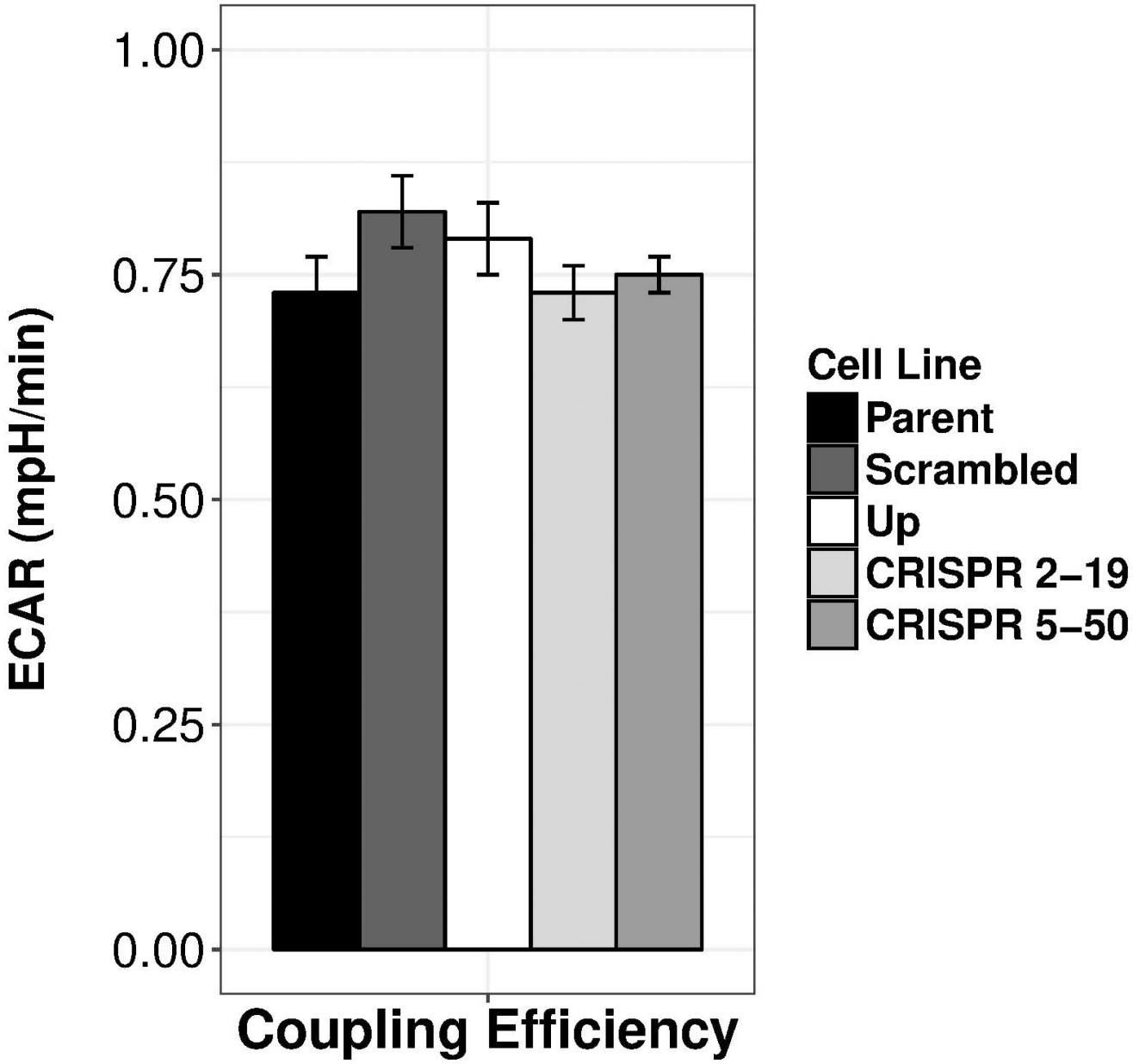

Figure 5: Coupling Efficiency

Coupling efficiency did not significantly differ between cell lines. Bars represent mean ± SEM. N=6. The *Parent* and *Scrambled* cell lines express parental NAT1 activity, the *Up* cell line expresses increased NAT1 activity, and the *CRISPR 2–19* and *CRISPR 5–50* cell lines express no NAT1 activity (knockout).

Table 1

Definition of Measurement Calculations and ANOVA *p*-value Summary Statistics

Measurement	Calculation	ANOVA *p*-value
Baseline OCR *	OCR after equilibration but before the injection of any compounds (mean of two measurements)	0.055
ATP-Linked OCR	(Minimium OCR after Oligomycin injection) – (Baseline OCR)	0.052
Reserve Capacity	(Maximum Mitochondria Capacity) – (Baseline OCR).	<0.0001
Proton Leak	(Minimium OCR after Oligomycin injection) – (Non-Mitochondrial Respiration)	0.021
Non-Mitochondrial Respiration	Minimum OCR after Rotenone/Antimycin A injection	0.229
Maximum Mitochondrial Capacity	(Maximum OCR measurement after FCCP † injection) – (Non-Mitochondrial Respiration)	<0.0001
Coupling Efficiency	ATP-linked OCR/baseline OCR	0.368
Baseline ECAR ‡	ECAR after equilibration but before the injection of any compounds (mean of two measurements)	<0.0001
Glycolytic Reserve Capacity	(Minimium ECAR after Oligomycin injection) – (Baseline ECAR)	<0.0001
Baseline OCR/ECAR	(Baseline OCR)/(Baseline ECAR)	0.011

* OCR = oxygen consumption rate

† FCCP = carbonyl cyanide-*p*-trifluoromethoxyphenylhydrazone

‡ ECAR= extracellular acidification rate